Theoretical Study of Complexes of Closo-Borane, Alane, and Gallane Anions with Cations of Light Metals Inside and Outside of Icosahedral Clusters [$A_{12}H_{12}^{2-}$] (A = B, Al, and Ga)

Oleg P. Charkin,*,†,‡,§ Nina M. Klimenko,†,§,|| Damian Moran,§ Alexander M. Mebel,*,† Dmitry O. Charkin,⊥ and Paul v. R. Schleyer*,§

Institute of Atomic and Molecular Sciences, Academia Sinica, P.O. Box 23-166, Taipei 10764, Taiwan, Institute of Problems of Chemical Physics, Russian Academy of Sciences, Chernogolovka, Moscow Region, 142432 Russia, Center of Computational Quantum Chemistry, University of Georgia, Athens, Georgia 30602-2525, Lomonosov Moscow State Academy of Fine Chemical Technology, Moscow, 117571 Russia, and Department of Chemistry, Lomonosov Moscow State University, Moscow, Russia

Received: June 12, 2002; In Final Form: September 16, 2002

Systematic B3LYP/6-31G* and B3LYP/6-311+G* calculations have been performed for families of closo-borane, alane, and gallane clusters consisting of $A_{12}H_{12}^{2-}$ (A = B, Al, and Ga) cages with endohedral or exohedral L^{n+} metal cations (L^{n+} = Li^+, Na^+, Cu^+, Be^{2+}, Mg^{2+}, Zn^{2+}, Al^+, Al^{3+}, Ga^+, and Ga^{3+}). Exohedral structure **1**, with tridentate cation coordination at an icosahedron face, is a global minimum for most species; bidentate coordination (structure **2**) is the transition state for cation migration around the dianion exterior. Migrational barriers (h_{migr}), which range from 3 to 5 kcal/mol for monocations and 10−15 kcal/mol for dications, increase with increased cation charge and increased cationic radius. $L^{n+}@B_{12}H_{12}^{2-}$ (L^{n+} = Li^+, Be^{2+}, Na^+, Mg^{2+}, Al^{3+}), $L^{n+}@Al_{12}H_{12}^{2-}$ (L^{n+} = Li^+, Na^+, Mg^{2+}, Al^+), and $L^{n+}@Ga_{12}H_{12}^{2-}$ (L^{n+} = Li^+, Na^+, Mg^{2+}, Ga^{3+}) endohedral clusters, with their cations located at the $A_{12}H_{12}^{2-}$ cage centers, are local I_h minima (**3**). Endohedral−exohedral isomer relative energies, E_{rel}(**3**/**1**), which are very high for the boranes, decrease rapidly down the borane−alane−gallane group and decrease along the He−Li^+−Be^{2+}−B^{3+} and Ne−Na^+−Mg^{2+}−Al^{3+} isoelectronic series. Endohedral isomers of gallane clusters with heavy multicharged cations are predicted to be most favorable in energy. Two types of transition structures for a **3** → **1** endohedral−exohedral rearrangement exist: cation exit through an edge and L^{n+} exit via a ruptured pentagonal "neck" of the cage. Li^+ and Be^{2+} borane salts prefer the former pathway, whereas Li^+, Na^+, and Mg^{2+} alane and gallane salts favor the latter mechanism. Cation exit barriers, h_{rear}, range from ∼15−55 kcal/mol and in an isoelectronic series decrease with increasing cation charge and increasing atomic mass. Endohedral $L^{n+}@A_{12}H_{12}^{2-}$ clusters show significant charge transfer from the anion to the cation; the hydrogen shell $[H]_{12}$ donates electrons to L^{n+} via the internal $[A]_{12}$ shell, which in many cases serves as an electron "conductor".

Introduction

The preparation, structure, and properties of polyhedral clusters with endohedral heteroatoms and ions, $X@A_n$, are intriguing. Ranging in size from large $Ln^{3+}@C_{60}$,[1a−g] (Sc, $Er)_3N@C_{80}$,[1h,i] $Sc_3N@C_{78}$[1j] and $Sc_2C_2@C_{84}$[1k] fullerene species to relatively compact aluminide (Al_{13}^-)[2a] and gallide (Ga_{13}^-)[2b] metal clusters, endohedral complexes elicit many special concerns. These include the valence state of endohedral atoms, the nature of the X−A_n interaction, and the thermodynamic and kinetic stability of these endohedral clusters.

Endohedral metal cage clusters, especially with transition metals, have been studied extensively. For example, there are numerous carbonyl complexes containing CFe_5, CRe_7, COs_9, NCo_6, PRh_9, $AsRh_{10}$, $SbRh_{12}$, and other moieties with interstitial carbon and pnictide atoms.[2c−e] Many atoms, both main group (H, Be, B, C, N, Al, Si, P) and transition metals, are capable of centering hexazirconium halide clusters and producing endohedral complexes with chemical properties that vary with the identity of their interstitial species.[2f] In ternary trielides (Tr = Al, Ga, In) with a $NaZn_{13}$ structure, endohedral encapsulating icosahedra have been found, linking Zintl compounds and intermetalics.[2g] In the past decade, a series of experimental and theoretical papers were devoted to gas-phase neutral and anionic aluminum clusters with various tri- and tetravalent heteroatoms inside the Al_{12} icosahedral cage (e.g., Al_{13}^-, CAl_{12}, $GeAl_{12}$, $PbAl_{12}$, etc).[2a,h−k] Many related endohedral clusters, including Tl_{13}^{11-}, $NiIn_{10}^{10-}$, $ZnIn_{10}^{8-}$, Ga_{13}^-,[1a] $Ga_{19}[C(SiH_3)_3]_6$,[2l] $SiAl_{14}(C_5Me_5)_6$,[2m] and $(AE)Sn_{12}^{2n-10}$ (AE = Ca or Sr) et cetera, have been characterized recently (see refs 3−5 for reviews). These clusters, including their condensed forms,[6a−c] represent an intermediate stage of matter between the chemistry of small, isolated polyatomic metal clusters and the chemistry of bulk metals.[6d]

Previously, we reported[7a,b] on icosahedral closo-borane, alane, and gallane dianions containing endohedral noble-gas atoms, $Ng@A_{12}H_{12}^{2-}$ (Ng = He, Ne, Ar, Kr; A = B, Al, Ga. $Al_{12}H_{12}^{2-}$ and $Ga_{12}H_{12}^{2-}$ cages were considered to be models for the recently synthesized dianions $Al_{12}R_{12}^{2-}$ [8] and $Ga_{12}H_{10}^{2-}$ [9] with bulky substituents R). DFT calculations showed that the I_h alane clusters were local minima with modest or small fragmentation

* Corresponding authors. E-mail: charkin@icp.ac.ru. mebel@po.iams.sinica.edu.tw. schleyer@chem.uga.edu.
† Academia Sinica.
‡ Russian Academy of Sciences.
§ University of Georgia, Athens.
|| Lomonosov Moscow State Academy of Fine Chemical Technology.
⊥ Lomonosov Moscow State University.

10.1021/jp021407o CCC: $22.00
Published on Web 10/25/2002

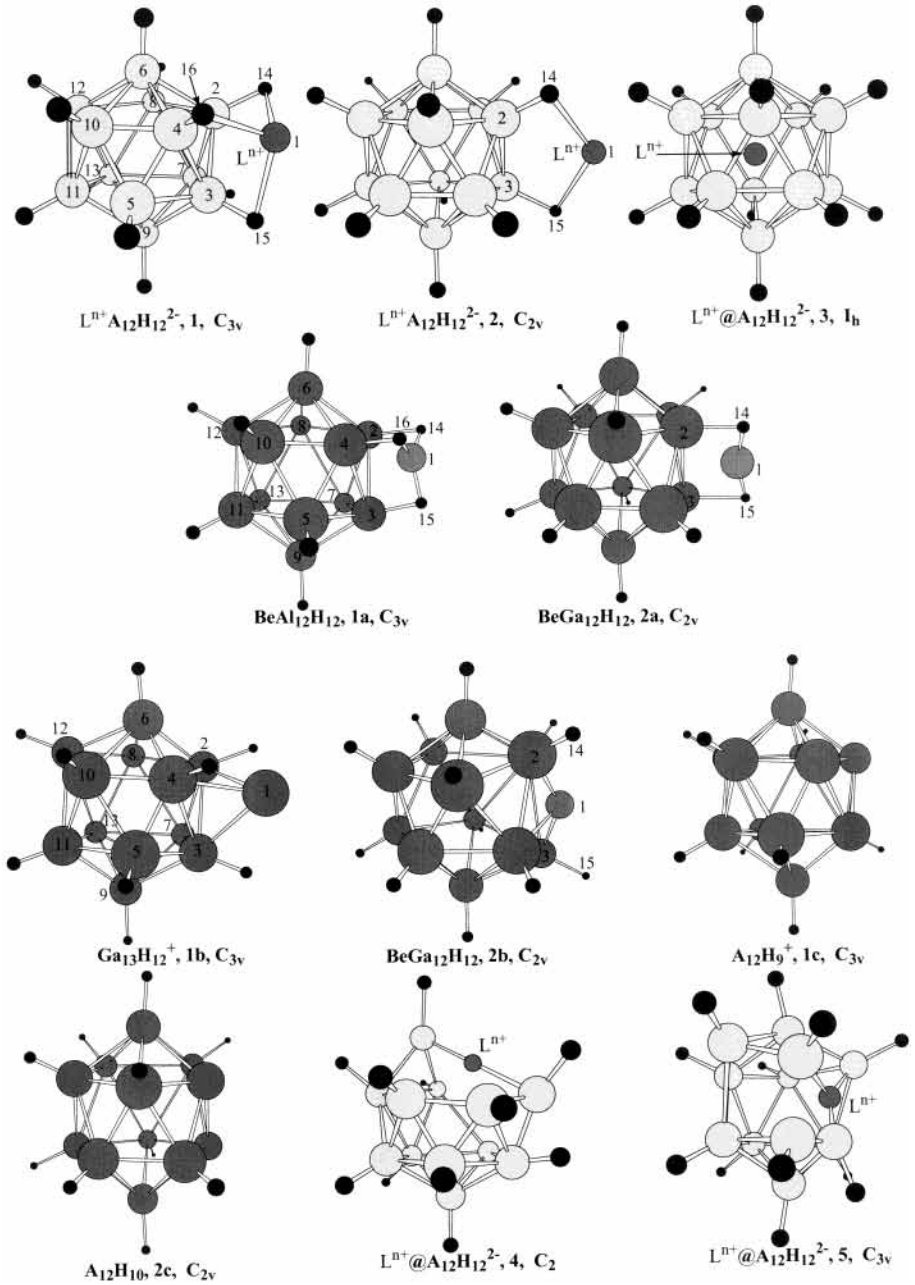

Figure 1. $L^{n+}\cdot A_{12}H_{12}^{2-}$ and $L^{n+}@[A_{12}H_{12}]^{2-}$ geometries.

barriers h_{exit} for the Ar and Kr endohedral complexes and large barriers for He and Ne. Interaction between the noble gases and the cage in $Ng@A_{12}H_{12}^{2-}$ was governed by the repulsion of their closed electronic shells, with minor charge transfer.

We now report related DFT calculations for closo-borane, alane, and gallane clusters $L^{n+}[A_{12}H_{12}]^{2-}$ (A = B, Al, Ga) complexed, either endohedrally or exohedrally, with $L^{n+} = Li^+$, Na^+, Cu^+, Al^+, Ga^+, Be^{2+}, Mg^{2+}, Zn^{2+}, Al^{3+}, and Ga^{3+} (integer values of the cation charges used here are formal because charge transfer in these clusters can be significant). Structures with the cations exohedrally (structures **1**, C_{3v}(t) and **2**, C_{2v}(b) in Figure 1) and endohedrally (structure **3**, I_h) coordinated have been considered. Whereas some clusters were examined previously (boranes in ref 10, alanes and gallanes in ref 11), their kinetic stability was not addressed. We now report barriers for the migration of exohedral cations over the surface of icosahedral cages, the relative energies of exohedral and endohedral configurations, and the barrier heights separating them. Furthermore, we investigate the nature of $A_{12}H_{12}^{2-}$ dianion deformation and polarization in the cation fields, determine the limits of exohedral and endohedral complex stability, and clarify the nature and role of charge transfer in these cation−cage interactions.

Computational Methods

As in our related work,[7,11] geometries (see Figure 1) were optimized using the hybrid density functional B3LYP method in conjunction with the 6-31G* basis set.[12] Borane and alane cluster structures were reoptimized with the more flexible 6-311+G* basis set. B3LYP/6-31G* vibrational frequencies and zero-point energies (ZPE) were then computed. B3LYP/6-31G* magnetic shielding constants (within the GIAO approach[13]) were computed for the borane and alane clusters.

Transition states (TS) for $L^{n+}B_{12}H_{12}^{2-}$ and $L^{n+}Al_{12}H_{12}^{2-}$ clusters also were located at the B3LYP/6-31G* level. However, the B3LYP/SDD approximation with the Stuttgart−Dresden effective core potential[14] was used to locate TS for the gallane clusters.

TABLE 1: Total Energies (au) and ZPE of $L^{n+}\cdot A_{12}H_{12}^{2-}$ (1), Relative Energies of the Endo Structure $L^{n+}@A_{12}H_{12}^{2-}$ (3), ZPE and Energy of Geometry Deformation of Cage $A_{12}H_{12}^{2-}$ by Inserted L^{n+} Ions, Barriers of Rearrangement of Endo Structure 3 to Exo Structure 1, and Relative Energies of Structures 2, 4, and 5 for Closo-Boranes, Alanes, and Gallanes (kcal/mol)[a]

(a) $L^{n+}\cdot B_{12}H_{12}^{2-}$

L^{n+}	Li^+	Be^{2+}	Na^+	Mg^{2+}	Al^{3+}	Al^+	Cu^+	Zn^{2+}	Ga^+
1, C_{3v}(t) E_{tot}	−313.3659	−320.4037	−468.1264	−505.7588	−547.7387	−548.2497	−1946.2938	−2084.9507	−2230.6763
ZPE	107.5	108.6	106.7	106.5	102.0	106.9	105.6	105.1	106.5
2, C_{2v}(b) E_{rel}[b]	5.1	13.2	4.3	10.0	-	4.5	4.3	6.2	5.0
3, I_h E_{rel}	117.0	55.4	351.6	251.3	155.5				
ZPE	106.9	105.8	98.8	99.5	98.6				
E_{def}	21.7	21.5	122.8	127.1	115.1				
h_{rear}	55.2	39.1	-	-	-				
4, C_2(b′) E_{rel}	43.1	32.1	−159.2	−130.0	−97.5				
5, C_{3v}(t′) E_{rel}	70.7	37.0	−79.6	−66.3	−53.1				

(b) $L^{n+}\cdot Al_{12}H_{12}^{2-}$ [c]

L^{n+}	Li^+	Be^{2+}	Na^+	Mg^{2+}	Cu^+	Ga^+	Al^{3+}
1, C_{3v}(t) E_{tot}	−2924.5015	−2931.5720	−3079.2721	−3116.9197	−4557.4443	−4841.8031	−3158.9646
ZPE	60.2	63.1	59.3	60.3	60.5	58.4	59.2
2, C_{2v}(b) E_{rel}[b]	2.4	11.9	2.8	10.8	3.4	2.0	13.9
3, I_h E_{rel}	23.7		59.7	37.9			
ZPE	59.1		58.8	53.7			
E_{def}	3.3		11.3	11.7			
h_{rear}	44.1		31.5	18.8			
4, C_2(b′) E_{rel}	52.3		27.7	13.1			
5, C_{3v}(t′) E_{rel}	52.6		38.9	18.8			

(c) $L^{n+}\cdot Ga_{12}H_{12}^{2-}$

L^{n+}	Li^+ [d]	Be^{2+} [e]	Na^+	Mg^{2+}	Ga^+	Ga^{3+}(b)[e]	Ga^{3+}(s)[e]	Al^{3+}(s)[e]
1, C_{3v}(t) E_{tot}	−23090.5540	−23097.6194	−23245.3191	23282.9629	−25005.9410	−25005.5234	−25005.5337	−23324.9943
ZPE	59.2	60.1	56.6	57.5	56.0	54.9	58.2	57.7
2, C_{2v}(b) E_{rel}[b]	4.4	9.2(b),36.9(s)[f]	4.2	10.2	4.3			
3, I_h E_{rel}	−0.8		53.3	−12.0			−82.8	
ZPE	59.2		59.9	59.5			71.2	

[a] Calculations of E_{tot} for boranes and alanes were performed at the B3LYP/6-311+G* level for structures **1** and **3** and at the B3LYP/6-311+G*//B3LYP/6-31G* level for structure **2**, whereas the other energies (ZPE, E_{def} h_{rear}, and E_{rel} for structures **4** and **5**) were calculated at the B3LYP/6-31G* level. For gallanes, all calculations were performed at the B3LYP/6-31G* level. Relative energies of structures **2** and **3** are calculated with respect to exo structure **1**, and the energies of structures **4** and **5** are calculated with respect to endo structure **3**. [b] Also referred to as h_{migr} in the text. [c] E_{tot} and ZPE for $Al^+@Al_{12}H_{12}^{2-}$ (**3**) with $N_{im} = 0$ are −3159.2948 au and 56.5 kcal/mol, respectively. Symmetric exohedral structures of $Al_{13}H_{12}^-$, **1**, C_{3v}(t), and **2**, C_{2v}(b) lie 50.5 and 48.4 kcal/mol lower in energy, respectively, than endohedral structure **3**, but both exhibit two imaginary frequencies. This result indicates that a nonsymmetric exohedral structure is expected to be the global minimum for $Al_{13}H_{12}^-$. [d] h_{rear} for $Li^+@Ga_{12}H_{12}^{2-}$ calculated at the B3LYP/6-31G* level with the SDD pseudopotential is 16.1 kcal/mol. [e] (b) and (s) denote "bridged" (**1** or **2**) and "skeleton" (**1b** or **2b**) types of structures, respectively. [f] Both external structures of $BeGa_{12}H_{12}$, **2** and **2b**, are local minima ($N_{im} = 0$).

All computations employed the Gaussian 98 program package.[15] The results are presented in Tables1−6 and in Figures 1−3.

Results and Discussion

Exohedral Structures 1 and 2. The most stable exohedral borane and alane isomers have the external cation L^{n+} tridentate coordinated to the $A_{12}H_{12}^{2-}$ cage face (structure **1**). The bidentate-coordinated structures (**2**) have a single b_1 imaginary frequency corresponding to the transition state for face−edge−face cation migration around the icosahedral cages ($BeGa_{12}H_{12}$ is exception, see below). The migrational barriers (h_{migr}) range from 2−5 kcal/mol for Li^+, Na^+, Al^+, Ga^+, and Cu^+ to 10−13 kcal/mol for Be^{2+}, Mg^{2+}, and Zn^{2+} and 13.9 kcal/mol for Al^{3+} in $Al_{13}H_{12}^+$ (Table 1). Among the cations, h_{migr} values are highest for the boranes, intermediate for the gallanes, and lowest for the alanes. The barriers increase with increasing cation charge and decrease down a group of the periodic table. The preference for tridentate structure **1** and the migrational nonrigidity of the clusters considered here are like the behavior of octahedral *closo*-$L^{n+}[B_6H_6^{2-}]$ and $L^{n+}[Al_6H_6^{2-}]$ salts[10c,10d,11] as well as numerous complex hydride and halide salts such as LMX_4 and LMX_6, which contain tetrahedral or octahedral anions.[16a,16b] The barrier for **1** → **2** → **1′** proton migration from one skeletal face to another via an edge in $Al_{12}H_{13}^-$ is about 15 kcal/mol lower than the barrier for the vertex exchange mechanism, which develops an AlH_2 group in the transition state.[11] Similarly, the **1** → **2** → **1′** mechanism dominates for cation migration in the $Al_{12}H_{12}^{2-}$ clusters, and this migrational

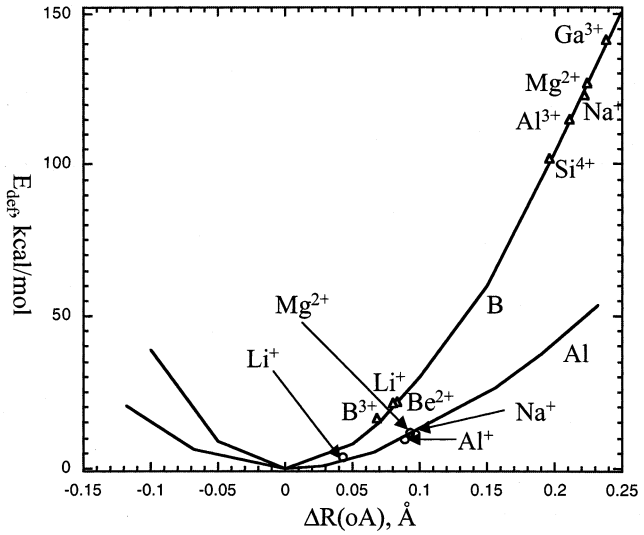

Figure 2. $A_{12}H_{12}^{2-}$ cage strain (E_{def}) due to endohedral L^{n+} encapsulation ($L^{n+}@[A_{12}H_{12}]^{2-}$) plotted against relative $A_{12}H_{12}^{2-}$ cluster expansion, ΔR(oA). E_{def} was calculated as the energy difference between the relaxed and deformed (without L^{n+}) cages. R(oA) is the distance between the center and a vertex of the $A_{12}H_{12}^{2-}$ icosahedron; ΔR(oA) is R(oA) relative to empty $A_{12}H_{12}^{2-}$.

nonrigidity should be observable by temperature-dependent NMR.

External Al^+, Ga^+, and alkali-metal monocations polarize $A_{12}H_{12}^{2-}$ polyhedra much less than a proton, but the qualitative effects are similar (see Table 2). The most favorable $BeAl_{12}H_{12}$ structure, **1a**, can be interpreted as an ion pair ($Al_{12}H_9^+ \cdot BeH_3^-$) between the beryllohydride anion and the $Al_{12}H_9^+$ closo-cation. A similar ion pair **1a** is obtained for Be^{2+}−gallane ($Ga_{12}H_9^+ \cdot BeH_3^-$) and $Al_{12}H_9^+ \cdot CuH_3^{2-}$, which have quasi-planar BeH_3^- and CuH_3^{2-} groups coordinated, respectively, above the $Al_{12}H_9$ cage faces (probably because of the high polarizing ability of Be^{2+} and Cu^+). $A_{12}H_{10} \cdot BeH_2$, with bidentate structure **2**, may be represented as a complex between the quasi-linear "molecule" BeH_2 and a "neutral" $A_{12}H_{10}$ cluster (**2a**). The cage distortions are even larger in systems with trications. For example, in $Al_{12}H_9^+ \cdot AlH_3$ (**1a**), the external Al is coordinated to the cage face atoms Al_2, Al_3, and Al_4 by short Al−Al bonds ($R(Al_1-Al_2) = 2.53$ Å), whereas in $Al_{12}H_9^+ \cdot BH_3$ (**1a**), the external BH_3 group is an inverted pyramid, with its three H atoms directed away from the cage.

These results indicate that closo-boranes, alanes, and gallanes may exist not only as traditional $A_{12}H_{12}^{2-}$ dianions but also as cations or neutral species lacking two or three peripheral H^- anions. Indeed, at B3LYP/6-31G* isolated $B_{12}H_9^+$ and $Al_{12}H_9^+$ cations (structure **1c**) and neutral $B_{12}H_{10}$ and $Al_{12}H_{10}$ (structure **2c**) are local minima with C_{3v} ($A_{12}H_9^+$) and C_{2v} ($A_{12}H_{10}$) symmetries. Compared to isolated $A_{12}H_{12}^{2-}$ dianions, the $[A]_{12}$ cages in **1c** and **2c** are compressed along the main axes. The formation of ion pairs or molecular complexes such as **1a** or **2a** occurs when the cage-hydrogens' shift from the cage to the cation is facilitated by the formation of a stable anion or a molecule such as BeH_3^- or BH_3. However, this process is reversed when Mg^{2+} is substituted for Be^{2+}; a pyramidalized MgH_3 group forms, and the bridging hydrogens shift from the cations back to a cage face. An alternative interpretation of **1a** and **2a** structures is that they are aggregated/segregated binary clusters, softened by a hydrogen shell.

$B_{12}H_{12}^{2-}$ dianion deformation is strongly anisotropic in the field of Al^{3+}, with barrierless transformation of **1a** into tridentate structure **1**. This is characteristic for monocation salts such as $Li^+ \cdot B_{12}H_{12}^{2-}$. Even more striking deformations were found for $Ga^{3+} \cdot Ga_{12}H_{12}^{2-}$ (**1**), in which the edges of the coordinated Ga_2-

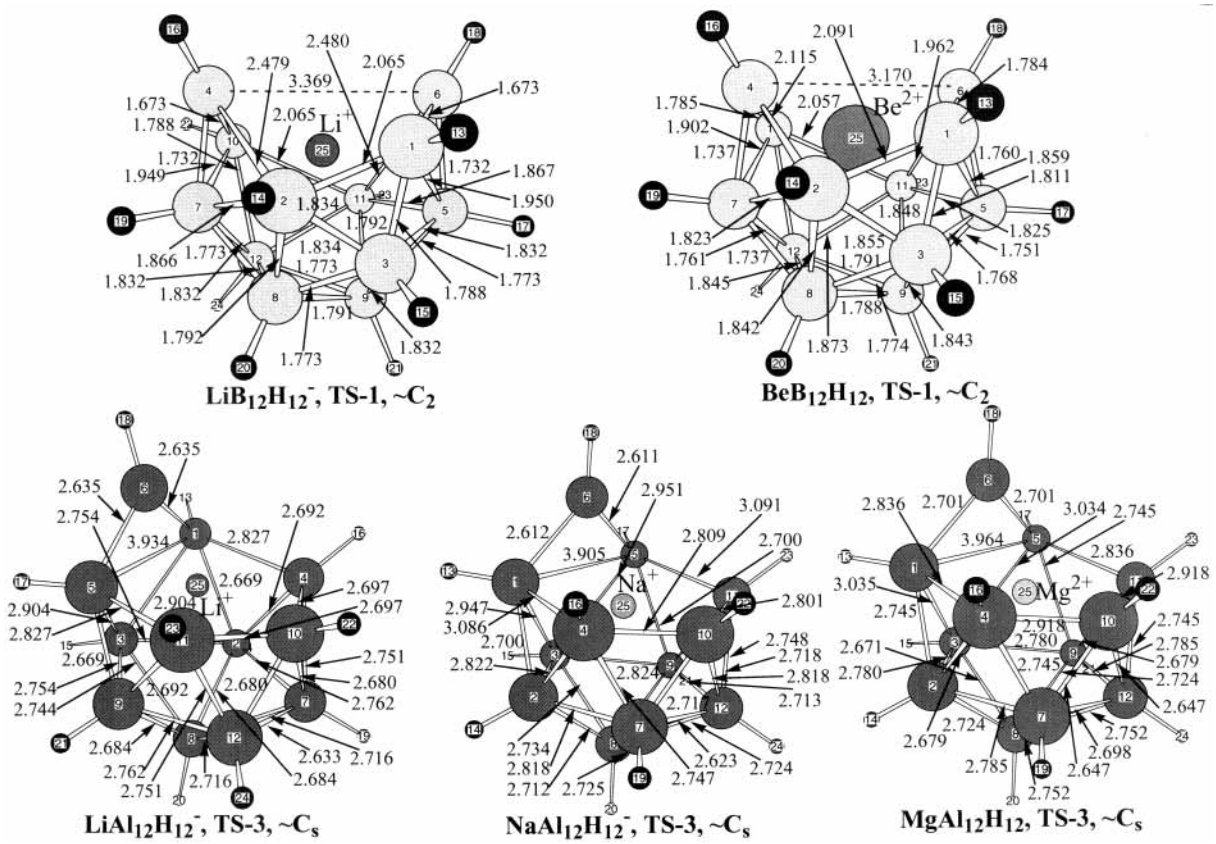

Figure 3. B3LYP/6-31G*-optimized transition structures for **3** → **1** rearrangements in $L^{n+}A_{12}H_{12}^{2-}$. Bond lengths are given in angstroms.

TABLE 2: Selected[a] Geometrical Parameters, Distances R (Å), and Angles φ (deg) of Closo-Boranes, Alanes, and Gallanes $L^{n+}\cdot A_{12}H_{12}^{2-}$ (1, C_{3v}(t))

(a) $L^{n+}\cdot B_{12}H_{12}^{2-}$

L^{n+}	Li^+	Be^{2+}	Na^+	Mg^{2+}	Al^+	Cu^+	Zn^{2+}	Ga^+	Al^{3+}
$R(L_1A_2)$	2.137	1.797	2.518	2.217	2.417	2.179	2.158	2.498	2.158
$R(A_2A_3)$	1.789	1.808	1.794	1.813	1.781	1.812	1.836	1.788	1.817
$R(L_1H_{14})$	1.900	1.545	2.203	1.956	2.107	1.973	1.973	2.197	1.889
$R(A_2H_{14})$	1.226	1.288	1.223	1.260	1.220	1.243	1.257	1.221	1.269
$\varphi(H_{14}L_1H_{15})$	101.8[b]	117.1[b]	88.0[b]	100.4[b]	91.1[b]	101.1[b]	102.8[b]	88.5[b]	103.3[b]
$\varphi(L_1H_{14}A_2)$	83.3	78.2	89.9	84.0	89.1	81.9	80.5	89.2	83.8

(b) $L^{n+}\cdot Al_{12}H_{12}^{2-}$

L^{n+}	Li^+	Be^{2+}	Na^+	Mg^{2+}	Al^{3+}	Cu^+	Ga^+
$R(L_1A_2)$	2.654	2.299	2.985	2.689	2.546	2.322	2.977
$R(A_2A_3)$	2.695	2.730	2.706	2.746	2.822	2.797	2.727
$R(L_1H_{14})$	1.984	1.471	2.538	1.904	1.659	1.723	2.547
$R(A_2H_{14})$	1.648	1.756	1.746	1.726	1.932	1.719	1.619
$\varphi(H_{14}L_1H_{15})$	112.9[b]	119.7[c]	103.3[b]	114.2[b]	120.0	120.0	103.2[b]
$\varphi(L_1H_{14}A_2)$	93.5	90.4	94.5	95.5	90.0	84.9	88.3

(c) $L^{n+}\cdot Ga_{12}H_{12}^{2-}$

L^{n+}	Li^+	Be^{2+}(b)	Be^{2+}(s)[d]	Na^+	Mg^{2+}	Ga^+	Ga^{3+}(b)	Ga^{3+}(s)	Al^{3+}(s)
$R(L_1A_2)$	2.601	2.254	2.176	2.928	2.643	2.828	2.829	2.430	2.474
$R(A_2A_3)$	2.592	2.644	3.757	2.606	2.633	2.615	2.757	4.055	4.037
$R(L_1H_{14})$	2.038	1.476	3.202	2.391	1.931	2.501	2.480	3.530	3.536
$R(A_2H_{14})$	1.617	1.746	1.542	1.608	1.708	1.580	1.575	1.540	1.540
$\varphi(H_{14}L_1H_{15})$	112.3[b]	119.7[c]	108.3[c]	102.5[b]	113.8[b]	104.7[b]	106.8[b]	119.0[c]	119.9[c]
$\varphi(L_1H_{14}A_2)$	90.0	68.4	36.9	92.0	93.0	84.5	25.4	34.9	36.5
$\varphi(A_2A_7A_3)$	60.7	62.3	92.0	61.0	62.0	61.2	67.3	95.2	95.5
$\varphi(A_{12}A_8A_{13})$	60.4	61.8	60.9	60.3	61.1	60.8	72.6	59.7	59.8

[a] Data for B3LYP calculations with the 6-311+G* basis set for boranes and alanes and 6-31G* for gallanes. Extension of the basis set to 6-311+G**does not affect the results significantly. [b] Atom L is located above hydrogen atoms H_{14}, H_{15}, and H_{16}. [c] Atom L is located between the plane $H_{14}-H_{15}-H_{16}$ and the coordinated face $A_2-A_3-A_4$ of the icosahedron $A_{12}H_{12}$. [d] $N_{im} = 2$.

Ga_3Ga_4 face and the opposite $Ga_{11}Ga_{12}Ga_{13}$ face are elongated relative to isolated $Ga_{12}H_{12}^{2-}$ by 0.18 and 0.41 Å, respectively. Significant opening of the face opposite the coordinated face is related to strong charge transfer from the dianion face to the triply charged cation (an "intraneutralization" or polarization "trans effect"). According to natural population analysis (NPA), electron density in the $Al^{3+}\cdot B_{12}H_{12}^{2-}$ (**1**) $B_{11}B_{12}B_{13}$ face decreases by ~0.6*e* compared with $B_{12}H_{12}^{2-}$, and the natural charge on Al is less than +2*e*.

In addition to **1**, isomer **1b** (C_{3v}) of gallane $Ga_{13}H_{12}^+$ and $AlGa_{12}H_{12}^+$ ions was found in which Ga^{3+} and Al^{3+} are inserted into the $[Ga]_{12}$ cage, thus converting the cages into a 13-vertex polyhedron. In contrast to "bridged" structure **1**, isomer **1b** is characterized by broken edges in the "attacked" face and strong (0.16 Å) elongation of the adjacent edges. Compared to isolated $Ga_{12}H_{12}^{2-}$, the face opposite the coordination site is essentially unchanged.

The vibrational spectra of closo-alane salts $L^{n+}\cdot Al_{12}H_{12}^{2-}$ (**1**) reveal that their bridging hydrogens are flexible. For example, separated by ~350 cm^{-1} in the spectrum of $MgAl_{12}H_{12}$, there are two intense doublets, $12a_1$ +19e and $13a_1$ +20e, that originate from $2t_{1u}$ and $3t_{1u}$ and are split by ~50 and 75 cm^{-1}, respectively (Table 3). In the long-wavelength doublet, which corresponds mostly to vibrations of the MgH_3 group, $\nu(12a_1)$ is lower than ν(19e), but in the short-wavelength doublet, which is related to the symmetric stretch of the $Al-H_b$ bonds, the order of frequencies is reversed [$\nu(13a_1) > \nu(20e)$], and $13a_1$ is much more intense than 20e. The interval, $\Delta\nu$, separating the doublets depends strongly on the cation charge and polarizing ability; $\Delta\nu$ decreases sharply when Mg^{2+} is substituted by Be^{2+} and nearly triples (up to ~1000 cm^{-1}) when Mg^{2+} is replaced by Li^+ or Na^+. For the salts incorporating cations of alkali and alkaline-earth metals, both doublets are predicted to be intense and should be the most characteristic features in the exohedral structure **1** IR spectra. In contrast to **1**, where frequencies of the bridged bonds are 300−600 cm^{-1} lower than those of the terminal bonds, all 12 highest frequencies of isomer **1b** (which has no bridging hydrogens) correspond to stretching ν(GaH) vibrations and lie within a narrow 30−70 cm^{-1} range.

Endohedral Structures 3, I_h. Differences among borane, alane, and gallane centrosymmetric endohedral structures $L^{n+}@A_{12}H_{12}^{2-}$ (**3**) are most clearly displayed in their configurational stability (Table 1). For the more spacious alane and gallane clusters, **3** is a local minimum only for $L^{n+}@Al_{12}H_{12}^{2-}$ ($L^{n+} = Li^+$, Na^+, Mg^{2+}, Al^+) and $L^{n+}@Ga_{12}H_{12}^{2-}$ ($L^{n+} = Li^+$, Na^+, Mg^{2+}, Ga^{3+}). $B_{12}H_{12}^{2-}$ has the smallest internal cavity (see also ref 10a); however, **3** is a local minimum on the PES for a broad range of borane-encapsulated cations ($L^{n+} = Li^+$, Be^{2+}, B^{3+}, Na^+, Mg^{2+}, Al^{3+}, Si^{4+}, Ga^{3+}). In contrast, transition-metal cations Cu^+ and Zn^+ do not favor central positions in the $A_{12}H_{12}^{2-}$ icosahedrons.

Table 1 shows that there is a clear trend in the energetic stabilization of **3** relative to that of **1** when going down the borane−alane−gallane group and when cation charge increases along the $He-Li^+-Be^{2+}-B^{3+}$ and $Ne-Na^+-Mg^{2+}-Al^{3+}$ isoelectronic series. ΔE_{rel}(**3**/**1**) drops from 60 (Na^+) to 38 (Mg^{2+}) kcal/mol for the alanes, whereas **3** is more stable than **1** by 1 (Li^+), 12 (Mg^{2+}), and 83 (Ga^{3+}) kcal/mol for the gallanes. In contrast to the boranes and alanes, endohedral gallane clusters (**3**) incorporating di- and trications are energetically favored over exohedral coordinations **1** and **2**. Extrapolating this trend, one may predict that the energetic preferences of endohedral

TABLE 3: Selected[a] Vibrational Frequencies ν_i (cm^{-1}) of Closo-Boranes, Alanes, and Gallanes $L^{n+}\cdot A_{12}H_{12}^{2-}$ (1, C_{3v}(t))

(a) Boranes
$L^{n+}\cdot B_{12}H_{12}^{2-}$

L^{n+}	Li^+	Be^{2+}	Na^+	Mg^{2+}	Al^+	Cu^+	Zn^{2+}	Ga^+	Al^{3+}
19e	1120 (22)	1241 (11)	1119 (28)	1172 (5)	1087 (22)	1102 (19)	1076 (7)	1080 (22)	1083 (2)
20e	2338 (116)	2047 (17)	2341 (166)	2109 (67)	2394 (1)	2169 (86)	2201 (12)	2400 (1)	2136 (3)
$12a_1$	1093 (90)	1223 (259)	1097 (651)	1075 (0)	1087 (87)	1067 (65)	1019 (32)	1081 (71)	991 (139)
$13a_1$	2380 (831)	2117 (395)	2383 (927)	2165 (378)	2439 (4)	2207 (623)	2222 (59)	2436 (71)	2145 (92)

(b) Alanes
$L^{n+}\cdot Al_{12}H_{12}^{2-}$

L^{n+}	Li^+	Be^{2+}	Na^+	Mg^{2+}	Al^{3+}	Cu^+	Ga^+
19e	662 (153)	1152 (0)	639 (190)	1016 (40)	655 (32)	948 (14)	564 (264)
20e	1618 (120)	1510 (85)	1638 (177)	1314 (107)	1602 (68)	1427 (48)	1753 (62)
$12a_1$	652 (167)	1368 (630)	605 (200)	965 (38)	901 (535)	1011 (135)	566 (263)
$13a_1$	1660 (1408)	1437 (46)	1669(1397)	1388 (1089)	1526 (26)	1472 (678)	1776 (434)

(c) Gallanes
$L^{n+}\cdot Ga_{12}H_{12}^{2-}$

L^{n+}	Li^+	Be^{2+}	Na^+	Mg^{2+}	Ga^+	Ga^{3+}(b)	Ga^{3+}(s)
19e	644 (136)	1032 (0)	623 (150)	945 (18)	567 (173)	514 (117)	573 (70)
20e	1613 (145)	1508 (74)	1643 (209)	1287 (123)	1794 (69)	1838 (26)	2039 (88)
$12a_1$	619 (220)	1275 (726)	588 (209)	905 (105)	567 (208)	560 (12)	568 (112)
$13a_1$	1651 (1413)	1438 (19)	1672 (1369)	1340 (948)	1816 (456)	1849 (138)	2041 (33)

[a] Data of B3LYP/6-31G* calculations. Intensities of vibrations (KM/mol) are given in parentheses.

TABLE 4: Calculated[a] Geometrical Parameters (Å) of Closo-Boranes, Alanes, and Gallanes $L^{n+}@A_{12}H_{12}^{2-}$ (3, I_h) with L Ions at the Center of the $[A_{12}]$ Icosahedron

L	empty[b]	Li^+	Na^+	Be^{2+}	Mg^{2+}	Al^{3+}	Ga^{3+}
			Borane				
R(B−L)	(1.700)	1.784	1.922	1.780	1.923	1.912	1.961
R(B−B)	1.787	1.876	2.021	1.872	2.022	2.010	2.062
R(B−H)	1.205	1.186	1.186	1.177	1.176	1.172	1.179
			Alane				
R(Al−L)	(2.571)	2.612	2.671		2.665	2.656	
R(Al−Al)	2.703	2.746	2.809		2.803	2.793	
R(Al−H)	1.605	1.586	1.587		1.574	1.598	
			Gallane				
R(Ga−L)	(2.453)	2.489	2.530		2.579		2.498
R(Ga−Ga)	2.579	2.616	2.659		2.712		2.626
R(Ga−H)	1.568	1.554	1.552		1.542		1.531

[a] Data of B3LYP calculations with the 6-311+G* basis set for boranes and alanes and 6-31G* for gallanes. [b] Data for isolated $A_{12}H_{12}^{2-}$ (calculations at the same level of theory, in parentheses: the distance from the center of icosahedron $A_{12}H_{12}^{2-}$ to vertex A).

structures versus those of exohedral structures will be even more pronounced for heavier In and Tl cages (in line with experimental findings: most known endohedral clusters consist of atoms located at the bottom of the periodic table).

As in endohedral noble-gas $Ng@A_{12}H_{12}^{2-}$ clusters,[7] the $L^{n+}@A_{12}H_{12}^{2-}$ cluster cage size, *R*(L−A), is linearly dependent on the inserted cation's atomic radius, *R*(L). Table 4 shows that the replacement of endohedral Li^+ with Na^+ or of Be^{2+} with Mg^{2+} leads to similar cage expansions, with *R*(A−L) increasing by 0.14 Å for boranes, 0.06−0.07 Å for alanes, and 0.04−0.05 Å for gallanes. In all clusters, the peripheral A−H bond lengths vary by less than 0.01 Å. Figure 2, which shows cage deformation energies, E_{def}, graphed as a function of the relative cage radius, *R*(o−A), reveals that $B_{12}H_{12}^{2-}$ and $Al_{12}H_{12}^{2-}$ in the borane and alane clusters are deformed like their related endohedral noble-gas complexes (see Figure 2 in ref 7). When L changes along an isoelectronic series such as $He-Li^+-Be^{2+}-B^{3+}$ or $Ne-Na^+-Mg^{2+}-Al^{3+}$, the cage radius *R*(L−A) varies only slightly (0.01−0.02 Å) because increased steric repulsion is compensated by increased cage-to-cation charge transfer. Meanwhile, the peripheral A−H bond lengths exhibit more-significant monotonic increases by up to 0.04 Å.

Skeletal A−A and peripheral A−H bond vibrational frequencies shift by just a few tenths of a cm^{-1} when Li^+ is replaced by Na^+ in endohedral alane and gallane clusters (Table 5). In contrast, the substitution of Li^+ with Na^+ and Be^{2+} with Mg^{2+} in boranes results in a significant ($\geq$100−200 cm^{-1}) decrease in these frequencies because of the extreme strain of the $B_{12}H_{12}$ cage when encapsulating second-row atoms. Two of four IR-active frequencies are expected to be informative for IR spectroscopic studies of endohedral $L^{n+}@A_{12}H_{12}^{2-}$ structures. In boranes, these intensive $2t_{1u}$ and $3t_{1u}$ modes lie in the range of 800−930 cm^{-1} and 1030−1190 cm^{-1}, respectively, whereas in alanes and gallanes, they appear between 300 and 400 cm^{-1} and 500 and 600 cm^{-1}, respectively.

Mulliken and NBO population analysis show that cation insertion leads to significant electron-density transfer from the $A_{12}H_{12}$ cage via two sets of the valence a_g and t_{1u} MOs. The first set has a dominant contribution from the cation's sp AO and the bonding MO of the $[A]_{12}$ skeleton. The second set of the a_g and t_{1u} MOs mostly corresponds to the A−H bonds. The "hydrogen shell" $[H]_{12}$ effective charge decreases by ~0.3−0.5*e* for the clusters with alkali cations and Mg^{2+} and by 1.0−1.2*e* for Be^{2+} clusters. Depending on the electronegativities of L and A and the external charge of the cluster, the electron density is distributed between L and the $[A]_{12}$ skeleton in various fractions. In $Li^+@B_{12}H_{12}^{2-}$, all $[H]_{12}$ charge (0.5*e*) is transferred to the cation, whereas the $[B]_{12}$ boron skeleton's charge changes only slightly. In contrast, $[H]_{12}$ electron density is mostly transferred to the $[B]_{12}$ skeleton in $Be@B_{12}H_{12}$, whereas the charge from $[H]_{12}$ is nearly equally distributed between the cation and the $[Al]_{12}$ cage in the Li^+ and Mg^{2+} alanes.

When the cation in structure **3** is varied along an isoelectronic series, the Q(AA) and Q(AH) overlap populations decrease and increase, respectively, in line with the decrease in skeletal vibrational frequencies and the increase in A−H stretching frequencies (see Tables 5). Overall, however, the $[A]_{12}$ inner-shell electron density changes only slightly, if at all. Where there is charge transfer from the anion to the cation, the external

TABLE 5: IR-Active[a] Vibrational Frequencies t_{1u} (cm^{-1}) of Closo-Boranes, Alanes, and Gallanes $L@A_{12}H_{12}^{2-}$ (3, I_h) with L Atoms at the Center of the $[A_{12}]$ Icosahedron

	B							Al					Ga			
L	empty[b]	Li^+	Na^+	Be^{2+}	Mg^{2+}	Al^{3+}	Ga^{3+}	empty[b]	Li^+	Na^+	Al^{3+}	Mg^{2+}	empty[b]	Li^+	Na^+	Mg^{2+}
t_{1u} 1		528	274	487	259	250	148	309	251	214	149	194	212	194	164	177
		(7)	(2)	(32)	(9)	(18)	(10)	(5)	(9)	(5)	(19)	(10)	(0)	(0)	(0)	(2)
2	710	933	915	801	880	802	835		383	382	336	364		412	300	408
	(7)	(9)	(37)	(3)	(13)	(2)	(8)		(10)	(13)	(6)	(22)		(1)	(4)	(4)
3	1089	1190	1033	1128	1059	1054	994	578	563	544	509	528	567	581	600	571
	(64)	(25)	(9)	(38)	(3)	(0)	(0)	(288)	(230)	(232)	(59)	(164)	(218)	(158)	(172)	(106)
4	2535	2692	2697	2771	2793	2831	2832	1810	1898	1897	1850	1956	1883	1986	2010	2057
	(1149)	(502)	(590)	(109)	(165)	(3)	(1)	(1656)	(1040)	(1102)	(1540)	(524)	(1656)	(1035)	(1041)	(483)

[a] Data of B3LYP/6-31G* calculations. Intensities of t_{1u} vibrations active in IR spectra (KM/mol) are given in parentheses. [b] Data for isolated $A_{12}H_{12}^{2-}$ (calculations at the same level of theory).

TABLE 6: Magnetic Shielding Constants σ (ppm)[a] for $A_{12}H_{12}^{2-}$ Closo Anions (A = B, Al) and $X@A_{12}H_{12}^{2-}$ Endo Clusters 3, I_h (X = Ng, L^{n+})

$X@A_{12}H_{12}^{2-}$	σ(B)	σ(X)	σ(H)	$X@A_{12}H_{12}^{2-}$	σ(Al)	σ(X)	σ(H)
$B_{12}H_{12}^{2-}$	127.0	(25.9)[b]	30.8	$Al_{12}H_{12}^{2-}$	575.2	(20.5)[b]	29.8
$He@B_{12}H_{12}^{2-}$	122.4	82.0	30.8	$He@Al_{12}H_{12}^{2-}$	572.9	78.2	29.8
				$Ne@Al_{12}H_{12}^{2-}$	575.6	400.2	29.7
$Li^+@B_{12}H_{12}^{2-}$	130.1	118.2	30.4	$Li^+@Al_{12}H_{12}^{2-}$	590.0	112.9	29.6
				$Na^+@Al_{12}H_{12}^{2-}$	588.9	530.6	29.5
$Be^{2+}@B_{12}H_{12}^{2-}$	138.2	140.6	29.7				
				$Mg^{2+}@Al_{12}H_{12}^{2-}$	620.0	616.6	29.1

[a] Calculated at the GIAO/B3LYP/6-31G* level. Absolute values of σ are presented. Calculations at the same level of theory give the following magnetic shielding constants (ppm): σ(Al) = 541 for AlH_4^- and σ(B) = 93.5 for B_2H_6, for which the accepted experimental NMR chemical shifts to the low field are δ(Al) = 100−103 and δ(B) = 16.6; L^{n+} isotropic shielding constants are the following: 95.1, 130.3, 622.7, and 694.0 ppm for Li^+, Be^{2+}, Na^+, and Mg^{2+} respectively. For exo structures **1**, σ values are the following: 90.3, 95.6, and 568.5 ppm for Li^+, Be^{2+}, and Na^+ in $L^{n+}\cdot B_{12}H_{12}^{2-}$, respectively, and 90.7 and 97.8 ppm for Li^+ and Be^{2+} in $L^{n+}\cdot Al_{12}H_{12}^{2-}$, respectively. σ(H) = 32.4 for TMS. [b] In parentheses, absolute shieldings (i.e., nucleus-independent chemical shifts, NICS,[17] without the signs reversed) computed at the centers of empty $A_{12}H_{12}^{2-}$ icosahedrons.

hydrogen shell $[H]_{12}$ serves as the main source of electron density, with the inner $[A]_{12}$ shell mostly acting as either an electron conductor or an electron acceptor. Significant differences in the vibrational spectra of exohedral and endohedral isomers of $L^{n+}A_{12}H_{12}^{2-}$ clusters may be used for their IR spectroscopic identification.

Magnetic Shielding Constants. We found earlier[7,11] that ^{3}He NMR absolute shieldings, σ(He), in $He@A_{12}H_{12}^{2-}$ clusters were larger than σ of ^{3}He in vacuo (upfield) and changed nonmonotonically along the $B_{12}H_{12}^{2-}-Al_{12}H_{12}^{2-}-Ga_{12}H_{12}^{2-}$ series. This result, together with the nonmonotonic behavior of the absolute shieldings computed in the center of free $A_{12}H_{12}^{2-}$ anions,[17] indicated that alanes were less aromatic than both boranes and gallanes.

Table 6 shows GIAO-B3LYP/6-31G* absolute magnetic shieldings, σ(L), for the cations in kinetically stable $L^{n+}@A_{12}H_{12}^{2-}$ borane and alane clusters and NICS of free $A_{12}H_{12}^{2-}$ borane and alane dianions. Like σ(He) in He-containing clusters, $\sigma(Li^+)$ and $\sigma(Be^{2+})$ in boranes and $\sigma(Li^+)$ in alanes are also larger than for free Li^+ and Be^{2+} cations. From boranes to alanes, $\sigma(Li^+)$ and σ(He) both decrease by 5 ppm, in line with the decrease in absolute shieldings at cage centers when comparing isolated $B_{12}H_{12}^{2-}$ to $Al_{12}H_{12}^{2-}$. These results indicate that the aromaticity of both clusters and noble-gas clusters decreases from boranes to alanes. Like the σ(Ne) behavior, the absolute shieldings of the heavier cations from the third period, $\sigma(Na^+)$ and $\sigma(Mg^{2+})$, are significantly smaller those for free cations (downfield).

In exohedral structures **1** both with light and heavy cations, $\sigma(L^{n+})$ is always smaller than that of free cations (downfield, Table 6). For light cations (such as Li^+ and Be^{2+}), the difference between $\sigma(L^{n+})$ values in endo (**3**) and exo structures (**1**) is significant (ca. 20 and 40 ppm, respectively), and that might be useful for the NMR spectroscopic identification of these isomers of clusters that are considered here.

Table 6 also reveals that the σ(A) and σ(H) absolute shieldings (and hence their chemical shifts) of endohedral clusters **3** change monotonically along the isoelectronic series $He-Li^+-Be^{2+}$ and $Ne-Na^+-Mg^{2+}$ but in opposite directions. σ(A) increases and σ(H) decreases because of the increase in charge transfer from the outer $[H]_{12}$ shell to the cation and partially to the inner $[A]_{12}$ shell (see above).

Transition States. As reported earlier,[7b] we performed a systematic search of the transition states (TS) of the endohedral exohedral rearrangement **3** → **1** for the borane and alane clusters using the B3LYP/6-31G* method. We investigated TS-1-, TS-2-, and TS-3-type transition states corresponding to the exit of the heteroatom from the cage via an edge, a triangular face, and a pentagonal "neck" of "a pot with its hinged lid opened", respectively. Optimized TS geometries for the clusters are shown in Figure 3, with the corresponding barriers (h_{rear}) relative to icosahedral structure **3** presented in Table 1.

As in $He@B_{12}H_{12}^{2-}$, the Li− and Be−borane cluster transition structures have C_2 symmetry and one imaginary frequency (230i and 265i cm^{-1}, respectively) and are of the TS-1 type (i.e., the cations exit from the cage via an edge). The cations are located inside the cage (endohedral structure) in both TS. Naturally, the exit of any of these metals via B_4-B_6 is accompanied by the rupture of the neighboring B_1-B_4 and B_6-B_{10} edges and by the elongation of the B_2-B_4 and B_6-B_{11} edges to ∼3.3 and 2.5 Å, respectively. The corresponding exit barriers, h_{rear} (with ZPE corrections), are 55.2 and 39.1 kcal/mol for $Li^+@B_{12}H_{12}^{2-}$ and $Be^{2+}@B_{12}H_{12}^{2-}$, respectively. By comparing these values with h_{exit} = 58.5 kcal/mol for $He@B_{12}H_{12}^{2-}$, one can see a clear trend of barrier decrease along the isoelectronic series $He-Li^+-Be^{2+}$, where charge increases and endohedral atom size decreases.

In contrast to boranes, the alane clusters (like the He and Ne alanes) have transition states of the the TS-3 type, which has "a pot with open lid" shape (Figure 3). As compared to structure

3, in TS-3, the triangular $Al_1-Al_6-Al_5$ lid together with the vertex group Al_6-H_{18} is thrown open, and the most favorable pathway for cation exit is through the uncovered quasi-planar pentagonal 1−4−10−11−5 neck. The cations in TS-3 are located below the neck plane (endohedral structure), except for Li^+, which practically lies in this plane.

Cage deformations in TS-3 are much larger than in TS-1. Besides the rupture of three of the five cage bonds connecting vertex Al_6 with its neighbors, a large number of other Al−Al bonds in the active hemisphere and in the equatorial area are either strongly elongated or broken. As a result, there is an additional large quadrangular 1−6−5−3 hole in the cage's side. In the opposite part of the cage most remote from this hole, two adjacent faces $Al_8-Al_7-Al_{12}$ and $Al_{10}-Al_7-Al_{12}$ are contracted by 0.05−0.10 Å so that their common edge Al_7-Al_{12} is shortened by 0.10 Å in comparison with the size of the isolated $Al_{12}H_{12}^{2-}$ dianion. The imaginary frequencies in TS-3 of all alanes vary in the 75−90i cm^{-1} range.

h_{rear} values for the alane clusters are 44.1 (Li^+), 31.5 (Na^+), and 18.5 (Mg^{2+}) kcal/mol. They are lower than h_{exit} in the isoelectronic $Ng@Al_{12}H_{12}^{2-}$ clusters (58.5 and 41.5 kcal/mol for He and Ne, respectively) but sufficiently high to ensure the kinetic stability of $Li^+@Al_{12}H_{12}^{2-}$, $Na^+@Al_{12}H_{12}^{2-}$, and (to a lesser extent) $Mg^{2+}@Al_{12}H_{12}^{2-}$. The h_{rear} barrier tends to decrease with heteroatom L down a subgroup in the periodic system and along an isoelectronic series with increasing size and charge. Moreover, the barrier heights in alanes show good qualitative correlation with relative energies E_{rel}(**4**/**3**) and E_{rel}(**5**/**3**) of the model "surface" structures **4**, C_2 and **5**, C_{3v} (Figure 1) where the heteroatom is fixed in the center of an edge or a face. For analogous systems, energies such as E_{rel}(**4**/**3**) and E_{rel}(**5**/**3**), which are easily obtained by partial optimization, should be useful in assessing the magnitude of h_{rear} before actual transition-state calculations. For other systems including Na-, Mg-, and Al-boranes, where **4** is much lower than **3**, one can also predict that their barriers h_{rear} and hence the kinetic stability of their endohedral structures **3** should be low.

Transition-state searches for the gallane clusters $L^{n+}@Ga_{12}H_{12}^{2-}$ at the same all-electron B3LYP/6-31G* level are hindered by computational difficulties. Hence, as for $Ng@Ga_{12}H_{12}^{2-}$,[7b] we performed Li^+−, Na^+−, Be^{2+}−, and Mg^{2+}−gallane TS calculations using the Stuttgart−Dresden effective core potential and B3LYP.[14] Parallel optimization of several alanes and gallanes at both the B3LYP/6-31G* and B3LYP/SDD levels demonstrated that the latter approach systematically overestimates interatomic distances by 0.20−0.25 Å and significantly underestimates vibrational frequencies and potential barriers. Therefore, the B3LYP/SDD results allow only qualitative conclusions regarding "entry" rearrangement barriers. For Li^+ and Na^+, exohedral-to-endohedral structural rearrangements (**1** → **3**) are more facile for the gallanes than the related alane clusters. As discussed above, **3** and **1** invert their relative position on the energy scale in gallanes with dications and trications, and their **3** → **1** "exit" rearrangement barriers increase sharply as compared to those of the related alanes. These gallane-cluster endohedral structures **3** are much more stable both energetically and kinetically and appear to be good prospects for synthesis.

Conclusions

Systematic B3LYP calculations of the family of closo-borane, alane, and gallane clusters with metal cations $L^{n+}A_{12}H_{12}^{2-}$ (A = B, Al, Ga; L^{n+} = Li^+, Na^+, Cu^+, Be^{2+}, Mg^{2+}, Zn^{2+}, Al^+, Al^{3+}, Ga^+, and Ga^{3+}) show that for most of them the global minimum on PES corresponds to "external" (exohedral) isomer **1** with a tridentate coordination of the cation at an icosahedral face. Bidentate structures **2** correspond to transition states for migration of the external cation around the anion along the face−edge−face pathways. The migrational barrier h_{migr} varies from 3 to 5 kcal/mol for single-charged cations to 10−15 kcal/mol for double-charged cations. In accord with the electrostatic considerations, h_{migr} increases with an increase of the cation charge and decreases with an increase of the cationic radius. The barriers in alanes are lower than those in related boranes and have intermediate values in gallanes. Because of the external cation field, the coordinated face of the $A_{12}H_{12}^{2-}$ anion expands, and its A−A bonds weaken, thus bridging hydrogen atoms are shifted toward the cation and the opposite face also expands. These deformations increase with the cation polarization propensity and structural nonrigidity of the anion.

In addition to traditional saltlike exohedral structures **1** or **2** of ionic pair $L^{n+}\cdot A_{12}H_{12}^{2-}$ with the $A_{12}H_{12}^{2-}$ dianion, several additional low-lying local minima were localized for the alanes and gallanes with multicharged cations of high polarizing ability (Be^{2+}, Al^{3+}, and Ga^{3+}). These new minima correspond to unusual isomers of three different types: (1) isomers **1a** (and **2a** for $BeGa_{12}H_{12}$) with a strong shift of three (or two) bridged H_b atoms from the coordinated face (or edge) of the cage to the cation, resulting in the formation of ionic pairs such as $BeH_3^-\cdot A_{12}H_9^+$ (or molecular complexes such as $BeH_2\cdot A_{12}H_{10}$) between the BeH_3^- anion (or BeH_2 molecule) and the closo cations $A_{12}H_9^+$ (or neutral $A_{12}H_{10}$); (2) isomers **1b** (and **2b** for $BeGa_{12}H_{12}$) in which the cation L^{n+} is inserted into the face (or edge) of the $A_{12}H_{12}^{2-}$ anion, completing the latter to 13-vertex polyhedron; (3) isomers with strong charge transfer from the cage to the triple-charged cation and with an expanded opposite face of the cage.

Besides exohedral isomers **1**, thirteen clusters (with Li^+, Be^{2+}, Na^+, Mg^{2+}, Al^{3+} for boranes; Li^+, Na^+, Mg^{2+}, Al^+ for alanes; and Li^+, Na^+, Mg^{2+}, Ga^{3+} for gallanes) were found to have another local minimum corresponding to I_h-symmetric endohedral isomer **3**, with the cation located in the center of the icosahedral $A_{12}H_{12}^{2-}$ cage. Relative energies of the endohedral isomer E_{rel}(**3**/**1**) vary from less than 60 kcal/mol for most of the alanes to 115 kcal/mol for $Li^+@B_{12}H_{12}^{2-}$ and 150−350 kcal/mol for boranes with cations from the second and third periods. E_{rel}(**3**/**1**) rapidly decreases in the boranes−alanes−gallanes group with an increase of the cation charge along the isoelectronic series He−Li^+−Be^{2+}−B^{3+} and Ne−Na^+−Mg^{2+}−Al^{3+}. In the gallane clusters with multicharged cations from the second and third periods, endohedral structures **3** are predicted to be more favorable energetically than exohedral structures **1** or **2**. The gallane clusters with endohedral structures with multicharged cations are prospects for experimental realization.

The endo−exo rearrangement **3** → **1** has two types of transition structures corresponding to the exit of the cation through an edge (TS-1) and through a pentagonal neck (TS-3) of the cage. These are like the TSs that were found earlier for the dissociation of endohedral clusters containing noble-gas atoms, $Ng@A_{12}H_{12}^{2-} \rightarrow Ng + A_{12}H_{12}^{2-}$. TS-1 (via an edge) is preferable for boranes with the lightest cations, Li^+ and Be^{2+}, whereas TS-3 (via a pentagonal neck) was located both for alanes and for gallanes with Li^+, Na^+, and Mg^{2+}. Calculated barriers h_{rear} are in the range of ∼15−55 kcal/mol and tend to decrease with an increase in the cation charge in isoelectronic series and with the replacement of the lightest Li^+ and Be^{2+} cations by their heavier analogues along periodic subgroups. The barriers for the other species, including $BeAl_{12}H_{12}$ and all boranes with cations from the second and lower periods, are

small, and their endohedral structures are predicted to be kinetically unstable.

It is worth noting that our results appeared to be stable with respect to the basis set expansion. For instance, when we enlarged the basis set to 6-311+G(3df,3pd) for single-point energy calculations of $LiAl_{12}H_{12}^-$, we found only a minor effect on the relative energies of structures **3**, **2**, and TS-3 with respect to that of **1** (23.8, 3.3, and 44.3 kcal/mol, respectively, at the B3LYP/6-311+G(3df,3pd) level vs 23.7, 2.4, and 44.1 kcal/mol within our regular B3LYP/6-311+G** approximation). For boranes, the effect of the basis set extension is expected to be even less significant. Similar B3LYP/6-311+G(3df,3pd) calculations would also be desirable for gallanes, but they are beyond the capability of our computational facilities.

In contrast to $Ng@A_{12}H_{12}^{2-}$, the $L^{n+}@A_{12}H_{12}^{2-}$ endohedral clusters have a significant ($\sim$0.5−1.2*e*) transfer of electron density from the anion to the cation. The external $[H]_{12}$ (hydrogen) shell serves as an electron donor, but the internal (skeletal) shell $[A]_{12}$ hardly changes its charge and in many cases can be regarded as an "electron conductor". This character of the charge transfer, $L^{n+} \leftarrow [A]_{12} \leftarrow [H]_{12}$, correlates with the behavior of the magnetic shieldings and, hence, the NMR chemical shifts, δ(A) and δ(H). Endohedral and exohedral isomers exhibit significant differences in vibrational spectra and chemical shifts of the cations δ(L), which might be used for their identification by IR and NMR spectroscopy.

Acknowledgment. This work is supported by Academia Sinica and the National Science Council of Taiwan, R.O.C., by grant no. NSC 8902113-M-001-069. O.P.C. and N.M.K thank the National Science Council of Taiwan, R.O.C., and Academia Sinica for their visiting fellowships at the Institute of Atomic and Molecular Sciences (grant no. NSC 91-2811-M-001-003) and also the University of Georgia for providing financial support and for their stay at the Center for Computational Quantum Chemistry.

Supporting Information Available: Detailed geometric parameters and vibration frequencies of exo- and endo-structures of closo-borane, alane, and gallane $L^{n+}\cdot A_{12}H_{12}^{2-}$ clusters. This material is available free of charge via the Internet at http://pubs.acs.org.

References and Notes

(1) (a) Shabtai, E.; Weitz, A.; Haddon, R. C.; Hoffman, R. E.; Rabinovitz, M.; Khong, A.; Cross, R. J.; Saunders, M.; Cheng, P.-C.; Scott, L. T. *J. Am. Chem. Soc.* **1998**, *120*, 6389. (b) Shimshi, R.; Cross, R. J.; Saunders, M. J. *J. Am. Chem. Soc.* **1997**, *119*, 1163. (c) Cross, R. J.; Saunders, M.; Prinzbach, H. *Org. Lett.* **1999**, *1*, 1479. (d) Bühl, M.; Thiel, W.; Jiao, H.; Schleyer, P. v. R.; Saunders, M.; Anet, F. A. L. *J. Am. Chem. Soc.* **1994**, *116*, 6005. (e) Cioslowski, J. *Chem. Phys. Lett.* **1994**, *227*, 361. (f) Bühl, M.; Thiel, W. *Chem. Phys. Lett.* **1995**, *233*, 585. (g) Hirsch, A.; Chen, Z.; Jiao, H. *Angew. Chem., Int. Ed.* **2000**, *39*, 3915. (h) Iezzi, E. B.; Duchamp, J. C.; Harish, K.; Glass, T. E.; Lee, H. M.; Olmstead, M. M.; Balch, A. L.; Dom, H. C. *J. Am. Chem. Soc.* **2002**, *124*, 524. (i) Olmstead, M. M.; de Bettencourt-Dias, A.; Duchamp, J. C.; Stevenson, S.; Marcia, D.; Dorn, H. C.; Balch, A. L. *J. Am. Chem. Soc.* **2000**, *122*, 12220. (j) Olmstead, M. M.; de Bettencourt-Dias, A.; Duchamp, J. C.; Stevenson, S.; Marcia, D.; Dorn, H. C.; Balch, A. L. *Angew. Chem., Int. Ed.* **2001**, *40*, 1223. (k) Wang, C. R.; Kai, T.; Tomiyama, T.; Yoshida, Y.; Kobayashi, Y.; Nishibori, E.; Takata, M.; Sakata, M.; Shinohara, H. *Angew. Chem., Int. Ed.* **2001**, *40*, 397.

(2) (a) Akola, J.; Manninen, M.; Hakkinen, H.; Landman, U.; Li, X.; Wang, L. S. *Phys. Rev. B* **1999**, *60*, R11297. (b) Corbett, J. D. *Inorg. Chem.* **2000**, *39*, 5178. (c) Ciani, G.; Sironi, A.; Martingendo, S.; Garlaschelli, L.; Della Pergola, R.; Zanello, P.; Laschi, F.; Masciocchi, N. *Inorg. Chem.* **2001**, *40*, 3905. (d) Wright, C. A.; Shapley, J. R. *Inorg. Chem.* **2001**, *40*, 6338. (e) Wright, C. A.; Brand, U.; Shapley, J. R. *Inorg. Chem.* **2001**, *40*, 4896. (f) Sun, D.; Hughbanks, T. *Inorg. Chem.* **2000**, *39*, 1964. (g) Nordell, K. J.; Miller, G. J. *Inorg. Chem.* **1999**, *38*, 579. (h) Rao, B. K.; Jena, P. *J. Chem. Phys.* **1999**, *111*, 1890. (i) Rao, B. K.; Jena, P. *J. Chem. Phys.* **2001**, *115*, 778. (j) Seitsonen, A. P.; Puska, M. J.; Alatalo, M.; Nieminen, R. M.; Milman, V.; Payne, M. C. *Phys. Rev. B* **1993**, *48*, 1981. (k) Kumar, V.; Bhattacharjee, S.; Kawazoe, Y. *Phys. Rev. B* **2000**, *61*, 8541. (l) Schnepf, A.; Stösser, G.; Schnöckel, H. *J. Am. Chem. Soc.* **2000**, *122*, 9178. (m) Purath, A.; Dohmeier, A.; Ecker, A.; Schnöckel, H.; Ahlrichs, R.; Stoermer, C.; Friedrich, J.; Jutzi, P. *J. Am. Chem. Soc.* **2000**, *122*, 6955. (n) Bobev, S.; Sevov, S. C. *Inorg. Chem.* **2001**, *40*, 5361.

(3) Cotton, F. A.; Wilkinson, G.; Murillo, C. A.; Bochman, M. *Advanced Inorganic Chemistry*, 6th ed.; Wiley & Sons: New York, 1999.

(4) (a) Corbett, J. D. *Struct. Bonding (Berlin)* **1997**, *87*, 157. (b) Seo, D. K.; Corbett, J. D. *Science (Washington, D.C.)* **2001**, *291*, 841.

(5) Braunstein, P.; Oro, L.; Raithby, P. R. *Metal Clusters in Chemistry*; Wiley-VCH: Berlin, 1999.

(6) (a) Schnepf, A.; Weckert, E.; Linti, G.; Schnöckel, H. *Angew. Chem., Int. Ed.* **1999**, *38*, 3381. (b) Linti, G.; Rodig, A. *Chem. Commun.* **2000**, 127. (c) Schnepf, A.; Schnöckel, H. *Angew. Chem., Int. Ed.* **2001**, *40*, 712. (d) Dohmeier, C.; Loos, D.; Schnöckel, H. *Angew. Chem., Int. Ed. Engl.* **1996**, *35*, 129.

(7) (a) Mebel, A. M.; Klimenko, N. M.; Moran, D.; Charkin, D. O.; Schleyer, P.v. R. *Russ. J. Inorg. Chem. (Engl. Transl.)* **2001**, *46*, 110. (b) Charkin, O. P.; Klimenko, N. M.; Moran, D.; Mebel, A. M.; Charkin, D. O.; Schleyer, P.v. R. *Inorg. Chem.* **2001**, *40*, 6913.

(8) (a) Hiller, W.; Klinkhammer, K.-W.; Uhl, W.; Wagner, J. *Angew. Chem., Ausg. B* **1991**, *103*, 182.

(9) Schnepf, A.; Stösser, G.; Köppe, R.; Schnöckel, H. *Angew. Chem., Int. Ed.* **2000**, *39*, 1637.

(10) (a) Jemmis, E. D.; Balakrishnarajan, M. M. *J. Am. Chem. Soc.* **2000**, *122*, 7392. (b) Mebel, A. M.; Najafian, K.; Charkin, O. P.; Schleyer, P. v. R. *J. Mol. Struct.: THEOCHEM* **1999**, *461*−*462*, 187. (c) Charkin, O. P.; Mebel, A. M. *Russ. J. Struct. Chem. (Engl. Transl.)*, **1989**, *30*, 6. (d) Mebel, A. M.; Charkin, O. P.; Kuznetsov, I. Yu.; Solntsev, K. A.; Kuznetsov, N. T. *Russ. J. Struct. Chem. (Engl. Transl.)* **1988**, *33*, 958.

(11) (a) Charkin, O. P.; Klimenko, N. M.; Schleyer, P.v. R. *Russ. J. Inorg. Chem. (Engl. Transl.)*, **2000**, *45*, 1539. (b) Moran, D.; Stahl, F.; Jemmis, E. D.; Schaefer, H. F., III; Schleyer, P. v. R. *J. Phys. Chem. A* **2002**, *106*, 5144-5154.

(12) (a) Becke, A. D. *J. Chem. Phys.* **1993**, *98*, 5648. (b) Lee, C.; Yang, W.; Parr, R. G. *Phys. Rev. B* **1988**, *37*, 785. (c) Hehre, W. J.; Radom, L.; Pople, J. A.; Schleyer, P. v. R. *Ab Initio Molecular Orbital Theory*; Wiley & Sons: New York, 1986. (d) Schleyer, P. v. R.; Allinger, N. L.; Clark, T.; Gasteiger, J.; Kollman, P. A.; Schaefer, H. F., III; Schreiner, P. R. *The Encyclopedia of Computational Chemistry*; Wiley & Sons.: Chichester, U.K., 1998.

(13) (a) Ditchfield, R. *Mol. Phys.* **1974**, *27*, 789. (b) Wolinski, K.; Hilton, J. F.; Pulay, P. *J. Am. Chem. Soc.* **1990**, *112*, 8251.

(14) (a) Dolg, M.; Wedig, U.; Stoll, H.; Preuss, H. *J. Chem. Phys.* **1987**, *86*, 866. (b) Dolg, M.; Stoll, H.; Preuss, H. *J. Chem. Phys.* **1989**, *90*, 1730. (c) Kaupp, M.; Schleyer, P. v. R.; Stoll, H.; Preuss, H. *J. Chem. Phys.* **1991**, *94*, 1360.

(15) Frisch, M. J.; Trucks, G. W.; Schlegel, H. B.; Scuseria, G. E.; Robb, M. A.; Cheeseman, J. R.; Zakrzewski, V. G.; Montgomery, J. A., Jr.; Stratmann, R. E.; Burant, J. C.; Dapprich, S.; Millam, J. M.; Daniels, A. D.; Kudin, K. N.; Strain, M. C.; Farkas, O.; Tomasi, J.; Barone, V.; Cossi, M.; Cammi, R.; Mennucci, B.; Pomelli, C.; Adamo, C.; Clifford, S.; Ochterski, J.; Petersson, G. A.; Ayala, P. Y.; Cui, Q.; Morokuma, K.; Malick, D. K.; Rabuck, A. D.; Raghavachari, K.; Foresman, J. B.; Cioslowski, J.; Ortiz, J. V.; Stefanov, B. B.; Liu, G.; Liashenko, A.; Piskorz, P.; Komaromi, I.; Gomperts, R.; Martin, R. L.; Fox, D. J.; Keith, T.; Al-Laham, M. A.; Peng, C. Y.; Nanayakkara, A.; Gonzalez, C.; Challacombe, M.; Gill, P. M. W.; Johnson, B. G.; Chen, W.; Wong, M. W.; Andres, J. L.; Head-Gordon, M.; Replogle, E. S.; Pople, J. A. *Gaussian 98*, revision A.7; Gaussian, Inc.: Pittsburgh, PA, 1998.

(16) (a) Charkin, O. P.; McKee, M. L.; Klimenko, N. M.; Schleyer, P. v. R. *Russ. J. Inorg. Chem. (Engl. Transl.)* **1998**, *43*, 1184. (b) Charkin, O. P.; McKee, M. L.; Klimenko, N. M.; Schleyer, P.v. R. *Russ. J. Inorg. Chem. (Engl. Transl.)* **1998**, *43*, 1520.

(17) Nucleus-independent chemical shifts (NICS) are based on computed absolute shieldings (σ). The signs are reversed to conform to the chemist's "chemical shift" (δ) sign convention, where the minus denotes upfield. See: (a) Schleyer, P. v. R.; Maerker, C.; Dransfeld, A.; Jiao, H.; van Eikema Hommes, N. J. R. *J. Am. Chem. Soc.* **1996**, *118*, 6317. (b) Schleyer, P. v. R.; Manoharan, M.; Wang, Z.-X.; Kiran, B.; Jiao, H.; Puchta, R.; Hommes, N. J. R. v. E. *Org. Lett.* **2001**, *3*, 2465.